



Enhanced Antitumor Efficacy by a Cascade of Reactive Oxygen Species Generation and Drug Release

Sheng Wang, Guocan Yu,* Zhantong Wang, Orit Jacobson, Li-Sen Lin, Weijing Yang, Hongzhang Deng, Zhimei He, Yuan Liu, Zhi-Yi Chen,* and Xiaoyuan Chen*

Abstract: Reactive oxygen species (ROS) can be used not only as a therapeutic agent for chemodynamic therapy (CDT), but also as a stimulus to activate release of antitumor drugs, achieving enhanced efficacy through the combination of CDT and chemotherapy. Here we report a pH/ROS dual-responsive nanomedicine consisting of β -lapachone (Lap), a pH-responsive polymer, and a ROS-responsive polyprodrug. In the intracellular acidic environment, the nanomedicine can realize pH-triggered disassembly. The released Lap can efficiently generate hydrogen peroxide, which will be further converted into highly toxic hydroxyl radicals via the Fenton reaction. Subsequently, through ROS-induced cleavage of thioketal linker, doxorubicin is released from the polyprodrug. In vivo results indicate that the cascade of ROS generation and antitumor-drug release can effectively inhibit tumor growth. This design of nanomedicine with cascade reactions offers a promising strategy to enhance antitumor efficacy.

Introduction

Reactive oxygen species (ROS) play important roles in biological processes; however, high levels of ROS can cause oxidative damage to cellular biomolecules (for example, lipids, proteins, DNA), resulting in cell death.^[1] Over the past decades, ROS-based strategies have shown great promise in cancer treatment.^[2] Photodynamic therapy (PDT), which employs photosensitizers to generate ROS under light activation, is a widely considered strategy for ROS-based tumor treatment.^[3] However, traditional PDT suffers from limited light penetration depth, restricting PDT to superficial

tumors.^[4] Compared to PDT, chemodynamic therapy (CDT) is an emerging therapeutic strategy that exploits biochemical reactions to generate ROS for tumor-cell killing.^[5] For example, the Fenton reaction is an iron-mediated reaction that can increase the ROS level by converting less-reactive hydrogen peroxide (H_2O_2) into hydroxyl radicals with significantly stronger oxidation capability.^[6] Therefore, CDT can avoid the above-mentioned disadvantage of PDT by excluding the need for external stimuli and can be used as an alternative strategy to traditional PDT.

ROS can be used not only as a therapeutic agent for CDT, but also as a stimulus to activate other treatment processes, achieving additive and even synergistic efficacies through the combination of CDT and other therapies. For example, ROS-responsive linkers, such as the diselenide bond, phenylboronic ester, peroxalate ester, and thioketal bond, have been explored to develop nanomedicines for antitumor-drug delivery.^[7] Triggered by ROS, the linkers are prone to be rapidly cleaved, enabling on-demand drug release. ROS-responsive nanomedicines offer higher selectivity than the commonly used pH- and glutathione-responsive nanomedicines because the ROS level in normal cells is relatively low.^[8] The two major methods to load drug molecules are physical encapsulation and chemical conjugation. However, encapsulated nanomedicines usually have unsatisfactory stability, resulting in inevitable drug leakage. To address this issue, polyprodrugs have been considered as an alternative strategy.^[9] By conjugating therapeutic drugs to polymer backbones through responsive linkers, polyprodrugs enable high drug-loading stability.^[10] Therefore, the development of polyprodrug-based nanomedicines capable of ROS generation and ROS-triggered drug release is a promising strategy to combine CDT with activated chemotherapy.

Herein, we report a pH/ROS dual-responsive nanomedicine that can achieve the cascade of ROS generation and antitumor-drug release. As shown in Figure 1, two types of amphiphilic polymers, pH-responsive poly(ethylene glycol) (PEG)-block-poly diisopropylaminoethyl methacrylate-block-poly dopamine (PEG-PDPA-PDA) and ROS-responsive PEG-block-poly thioketal doxorubicin (DOX) prodrug (PEG-PtkDOX), were synthesized to form nanomedicines (NMs) as well as encapsulate β -lapachone (Lap) and ferric ions (Fe^{3+}). The as-prepared pH/ROS dual-responsive nanomedicine (denoted as PtkDOX-NM) can achieve effective tumor accumulation via the enhanced permeability and retention (EPR) effect. Thereafter, in the intracellular acidic environment, the pH-triggered hydrophobic-to-hydrophilic transition of PDPA segments leads to disassembly of the

[*] Dr. S. Wang, Dr. Z. Y. Chen

Department of Ultrasound Medicine,
 Laboratory of Ultrasound Molecular Imaging,
 The Third Affiliated Hospital of Guangzhou Medical University,
 The Liwan Hospital of the Third Affiliated Hospital of
 Guangzhou Medical University
 Guangzhou, Guangdong 510000 (China)
 E-mail: winchen@vip.126.com

Dr. S. Wang, Dr. G. Yu, Dr. Z. Wang, Dr. O. Jacobson, Dr. L. S. Lin,
 Dr. W. Yang, Dr. H. Deng, Dr. Z. He, Dr. Y. Liu, Prof. X. Chen
 Laboratory of Molecular Imaging and Nanomedicine,
 National Institute of Biomedical Imaging and Bioengineering,
 National Institutes of Health, Bethesda, MD 20892 (USA)
 E-mail: guocan.yu@nih.gov
 shawn.chen@nih.gov

 Supporting information and the ORCID identification number(s) for the author(s) of this article can be found under:
 <https://doi.org/10.1002/anie.201908997>

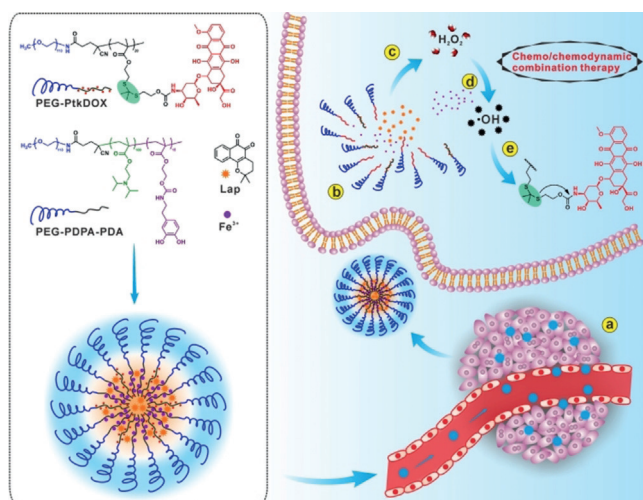


Figure 1. Schematic illustration showing the cascade of ROS generation and drug release. a) The nanosized PtkDOX-NMs can accumulate in tumor tissue via the EPR effect. b) In the acidic endosome environment, due to the pH-induced hydrophobic-to-hydrophilic transition of the PDPA segments, the PtkDOX-NMs can realize pH-triggered disassembly and rapid release of Lap. c) The released Lap can generate H_2O_2 . d) In the presence of iron ions, highly toxic hydroxyl radicals can be produced through the Fenton reaction, resulting in amplified ROS level inside cells. e) The produced hydroxyl radicals can further trigger antitumor drug release for chemo/chemodynamic combination therapy.

PtkDOX-NMs and rapid release of Lap.^[11] Nicotinamide adenine dinucleotide (phosphate):quinone oxidoreductase 1 (NQO1), which is overexpressed in tumor cells, catalyzes the generation of H_2O_2 through futile redox cycles of Lap.^[12] H_2O_2 is further converted into highly toxic hydroxyl radicals via the Fenton reaction. The hydroxyl radicals can cause not only oxidative damage to tumor cells, but also promote DOX release from the polyprodrug through ROS-induced cleavage of the thioketal linker. The PtkDOX-NMs show the following distinct features: i) the polyprodrug allows high loading stability; ii) Lap realizes tumor-specific intracellular ROS generation; iii) the cascade of ROS generation and antitumor drug release achieves enhanced antitumor efficacy through chemo/chemodynamic combination therapy.

Results and Discussion

The monomers containing thioketal linker (**M1** and **M2**) were first synthesized (Supporting Information, Scheme S1). A similar monomer without the thioketal linker (**M3**) was also synthesized and used as a non-responsive control (Supporting Information, Scheme S2). Then the polymers were synthesized through reversible addition fragmentation chain transfer polymerization.^[13] Subsequently, DOX was conjugated to the polymers to obtain the amphiphilic polyprodrugs, ROS-responsive PEG-PtkDOX and non-responsive PEG-PDOX (Supporting Information, Schemes S3 and S4). The pH-responsive polymer containing dopamine groups, PEG-PDPA-PDA, was also synthesized (Supporting Information, Scheme S5). NMR spectroscopy and gel permeation chroma-

tography results confirmed the successful synthesis of the monomers and polymers (Supporting Information, Figures S1–S11). In the absorption spectra of PEG-PtkDOX and PEG-PDOX, the typical absorbance peak of DOX at a wavelength of 480 nm was observed, indicating the successful conjugation of DOX to form the polyprodrugs (Supporting Information, Figure S12). According to the standard curve, the DOX content of PEG-PtkDOX was 44.4% (Supporting Information, Figure S13).

Then the PtkDOX-NMs with spherical morphology and a diameter of around 60 nm were prepared by coassembly of PEG-PtkDOX and PEG-PDPA-PDA (Figure 2a). The Lap

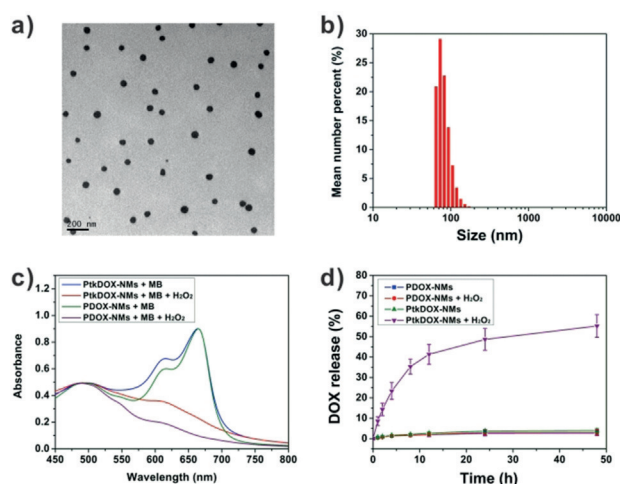


Figure 2. a) Transmission electron microscopy image of the PtkDOX-NMs. b) Effective particle diameter of the PtkDOX-NMs determined by dynamic light scattering. c) Absorption spectra of different samples with MB in the absence or presence of H_2O_2 . d) In vitro release profiles of DOX from PDOX-NMs and PtkDOX-NMs in the absence or presence of H_2O_2 .

was encapsulated into the hydrophobic core of the nanomicelle; while ferric ions were chelated by DOX and dopamine groups through non-covalent coordination interactions. The hydrodynamic diameter of PtkDOX-NMs was 76.9 ± 15.9 nm (Figure 2b). Moreover, the PtkDOX-NMs showed good colloidal stability, which made them suitable for in vivo applications (Supporting Information, Figure S14).^[14] The control group (denoted as PDOX-NMs) assembled from PEG-PDOX and PEG-PDPA-PDA showed similar morphology and hydrodynamic diameter to PtkDOX-NMs (Supporting Information, Figures S15 and S16). Then the pH-responsiveness of the PtkDOX-NMs to the acidic environment was evaluated. As shown in Figure S17 in the Supporting Information, upon incubation at pH 6.0, the PtkDOX-NMs rapidly disintegrated, indicating the pH-triggered disassembly of the PtkDOX-NMs. This pH-triggered disintegration of particles accelerated the release of Lap, as evidenced by the boost release at pH 6.0, which was in sharp contrast with that at pH 7.4 (Supporting Information, Figure S18). Then the generation of hydroxyl radicals was evaluated by using an indicator for hydroxyl radicals. As shown in Figure 2c, in the presence of H_2O_2 , both PtkDOX-

NMs and PDOX-NMs can lead to a decrease in absorbance of methylene blue (MB), demonstrating the degradation of MB by the hydroxyl radicals. To examine the cascade of hydroxyl-radical generation and drug release, the DOX release behaviors of PtkDOX-NMs and PDOX-NMs were measured *in vitro* (Figure 2d). In the absence of H_2O_2 , the PtkDOX-NMs showed extremely high stability without obvious drug leakage. However, 55.2% of DOX was released from PtkDOX-NMs in the presence of H_2O_2 after 48 h of incubation. In contrast, negligible DOX release was observed in the PDOX-NMs group. The ROS-triggered DOX release was attributed to the hydroxyl-radical-induced cleavage of the thioketal linker (Figure 1).

To investigate the intracellular H_2O_2 generation by Lap, a NQO1-overexpressing A549 cell line was used. After a 2 h incubation with Lap, the cells were stained with 2',7'-dichlorofluorescein diacetate (an ROS probe). As shown in the flow cytometry analysis (Supporting Information, Figure S19), fluorescence intensities inside cells increased with increasing Lap concentration, demonstrating that the ROS level inside cells was significantly increased. However, in the presence of dicoumarol (a NQO1 inhibitor), the function of Lap was blocked (Supporting Information, Figure S20). Furthermore, the addition of Lap did not have an obvious impact on the intracellular ROS level of 293T cells, which express NQO1 at a low level (Supporting Information, Figure S21). These results demonstrated that the Lap-induced ROS amplification is dependent on NQO1. Considering the NQO1-overexpression in various cancer cells, the Lap-based system shows high selectivity for cancer cells over normal cells. Excitingly, the coexistence of Lap and iron ions showed significantly enhanced oxidation capability (Supporting Information, Figure S22), attributing to the efficient conversion of H_2O_2 into more active hydroxyl radicals via the Fenton reaction.

Then the cellular uptake and drug distribution were investigated on A549 cells using confocal laser scanning microscopy (CLSM). As shown in Figure 3, the free DOX could quickly enter cells and diffuse into the nucleus, resulting

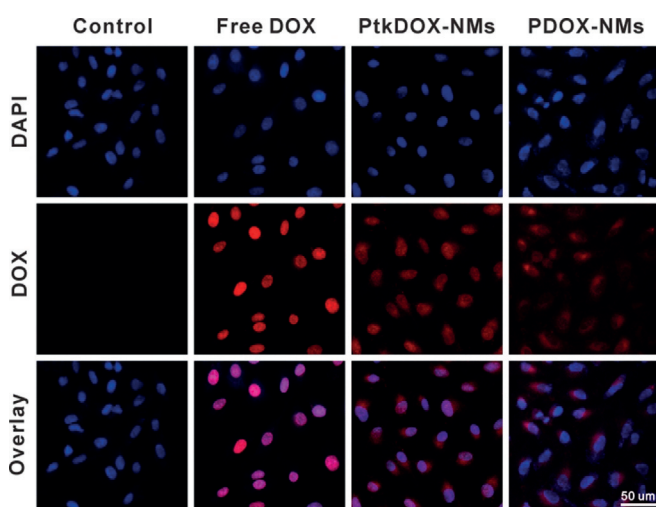


Figure 3. CLSM images of A549 cells upon incubation with free DOX, PtkDOX-NMs, and PDOX-NMs for 6 h. DOX concentration: 10 mg L^{-1} .

in the appearance of strong red fluorescence inside the nucleus. For the cells treated with PDOX-NMs, almost no red fluorescence could be detected in the nuclei, which demonstrated that DOX was not released from the PDOX-NMs. In contrast, PtkDOX-NMs-treated cells exhibited obvious DOX distributions in both the nucleus and the cytoplasm, indicating ROS-triggered drug release from the PtkDOX-NMs. Then the antitumor activities of free DOX and the different nanomedicines were evaluated by methyl thiazolyl tetrazolium assay. The blank nanomedicines without the polydrug (denoted as NMs) were used as control groups. As shown in Figure 4a, in the absence of Lap, all the nanoformulations

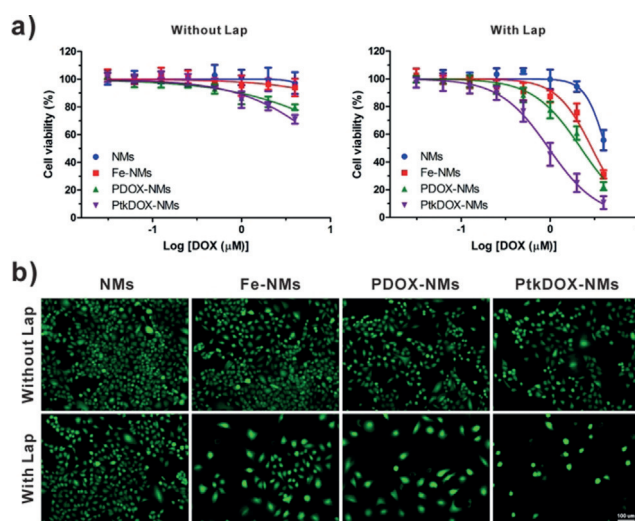


Figure 4. a) Viability of A549 cells incubated with different samples for 48 h. b) Fluorescence images of A549 cells after treatments (DOX concentration: $2 \times 10^{-6} \text{ M}$) and Calcein AM staining.

showed low cytotoxicities; however, the Lap-loaded nanoformulations showed obvious antitumor effects. This result indicated that Lap was critical to the generation of ROS and the acceleration of drug release. Compared with the Lap-loaded NMs, the NMs loaded with Lap and Fe^{3+} exhibited higher cytotoxicity, which was attributed to the conversion of H_2O_2 to highly toxic hydroxyl radicals. Furthermore, the ROS-responsive PtkDOX-NMs showed much higher antitumor activity compared with the PDOX-NMs, because of the cascade of ROS generation and drug release. This chemo/chemodynamic combination therapy effect was also confirmed by a live-cell staining assay. Compared with the control groups, fewer living cells were observed after the PtkDOX-NMs treatment, confirming the most potent antitumor capability of the PtkDOX-NMs (Figure 4b).

The *in vivo* performance of PtkDOX-NMs was further investigated by positron emission tomography (PET) imaging on A549-tumor-bearing mice. Deferoxamine was conjugated to the PtkDOX-NMs to chelate with the radionuclide zirconium-89 (^{89}Zr). The decay-correlated PET images of mice ($n = 5$) intravenously injected with ^{89}Zr -PtkDOX-NMs were acquired at different time points postinjection. Upon the injection of ^{89}Zr -PtkDOX-NMs, the tumor signal intensity gradually increased, indicating effective tumor accumulation

of the ^{89}Zr -PtkDOX-NMs (Figure 5a). Quantitative three-dimensional volume-of-interest analysis was used to measure the tumor uptake efficiency. The tumor uptake reached the maximum value of $5.89\% \text{ID g}^{-1}$ at 24 h postinjection (Fig-

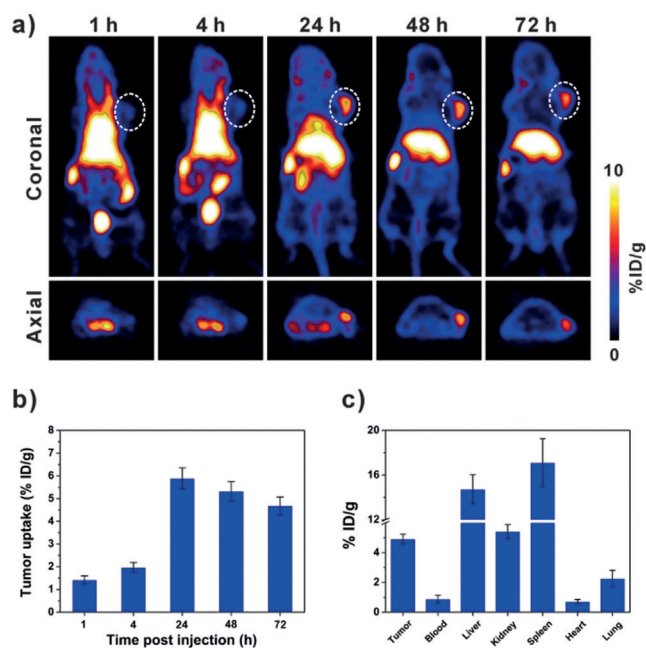


Figure 5. a) PET images of mice intravenously injected with ^{89}Zr -PtkDOX-NMs. b) Tumor uptake of the ^{89}Zr -PtkDOX-NMs at different time points ($n=5$). c) Biodistribution of tumor and primary organs at 72 h postinjection.

ure 5b). Thereafter, the tumor accumulation slightly dropped to $4.68\% \text{ID g}^{-1}$ at 72 h time point. The high tumor uptake was mainly attributed to the prolonged blood circulation and the EPR effect (Supporting Information, Figure S23). After 72 h postinjection, the mice were euthanized. The ex vivo biodistribution result measured by using γ -counting further confirmed the effective tumor accumulation and retention of ^{89}Zr -PtkDOX-NMs (Figure 5c).

Encouraged by the outstanding in vivo performance, the antitumor performance of PtkDOX-NMs was further evaluated on A549-tumor-bearing mice. Free DOX or nanomedicines were intravenously injected into mice every 3 d. The mice administrated with free DOX or nanomedicine exhibited obvious therapeutic effects (Figure 6a). Particularly, compared to other groups, the PtkDOX-NMs showed the highest inhibition of tumor growth. After 21 d of observation, the tumors of different groups were collected and weighed. The average tumor weight of the PtkDOX-NMs group was only 0.187 g, which was much lower than those of the other groups (Figure 6b). Moreover, the histological analysis results further confirmed the most efficient therapeutic effect of the chemo/chemodynamic combination therapy group (Figure 6c and Supporting Information, Figure S24). This enhanced antitumor efficacy was attributed to the cascade of hydroxyl-radical generation and drug release. It should be emphasized that the systemic toxicity was remarkably inhibited by fully taking advantage of nanotechnology and

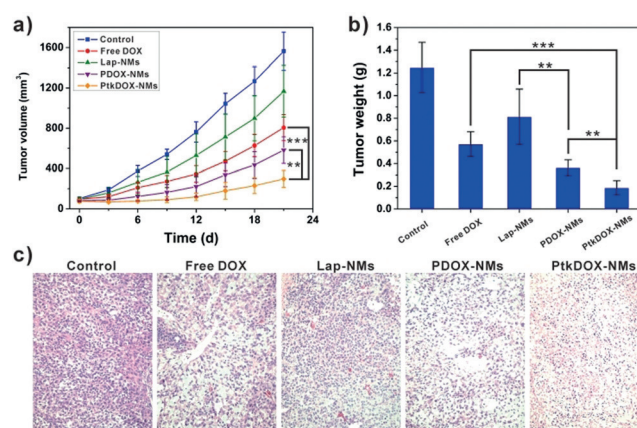


Figure 6. a) Tumor growth curves of the mice treated with different samples. b) Tumor weights of different groups after treatment. $**p < 0.01$, $***p < 0.001$. c) Hematoxylin and eosin (H&E) analyses of tumor tissues after different treatments.

rational design, no significant body weight loss or noticeable organ damage was caused by the treatment of PtkDOX-NMs (Supporting Information, Figures S25 and S26).

Conclusion

In conclusion, we have developed a nanomedicine consisting of pH-responsive polymer and an ROS-responsive polyprodrug, in which Lap and ferric ions were loaded. The nanosized structure and excellent colloidal stability enabled high tumor accumulation and retention. In acidic intracellular environment, the nanomedicine could realize pH-induced disassembly and subsequent Lap release. The H_2O_2 specifically produced in cancer cells by Lap could be further converted to highly toxic hydroxyl radicals via the Fenton reaction, resulting in elevated ROS levels inside cells. The ROS promoted the release of active DOX through cleavage of the thioketal linker. Therefore, chemo/chemodynamic combination therapy could be achieved by the cascade of ROS generation and drug release. Both in vitro and in vivo experiments demonstrated the potent antitumor activity and low systemic toxicity of this nanomedicine. This study provides a strategy for designing nanomedicine with high selectivity for cancer cells and enhanced antitumor efficacy.

Acknowledgements

This work was supported by the National Natural Science Foundation of China (No. 81671707), Natural Science Foundation of Guangdong Province (No. 2016A030311054), Research Projects of Guangzhou Science Technology and Innovation Commission (No. 201607010201), Research Fund for Lin He's Academician Workstation of New Medicine and Clinical Translation, Higher Education Colleges and Universities Innovation Strong School Project (Q17024072), Research Fund of National Education Steering Committee for Graduates in Medical Degree (B3-20170302-06) and the

Intramural Research Program (IRP) of the National Institute of Biomedical Imaging and Bioengineering (NIBIB), National Institutes of Health (NIH). We thank Dr. Vincent Schram in the NICHD Microscopy Imaging Core for technical support.

Conflict of interest

The authors declare no conflict of interest.

Keywords: cancer therapy · drug delivery · Fenton reaction · nanomedicine · prodrugs

How to cite: *Angew. Chem. Int. Ed.* **2019**, *58*, 14758–14763
Angew. Chem. **2019**, *131*, 14900–14905

- [1] a) Z. Zhou, J. Song, L. Nie, X. Chen, *Chem. Soc. Rev.* **2016**, *45*, 6597–6626; b) S. S. Sabharwal, P. T. Schumacker, *Nat. Rev. Cancer* **2014**, *14*, 709–721; c) R. Rodriguez, R. Redman, *Proc. Natl. Acad. Sci. USA* **2005**, *102*, 3175–3176.
- [2] a) L. Cheng, C. Wang, L. Feng, K. Yang, Z. Liu, *Chem. Rev.* **2014**, *114*, 10869–10939; b) Z. Tang, Y. Liu, M. He, W. Bu, *Angew. Chem. Int. Ed.* **2019**, *58*, 946–956; *Angew. Chem.* **2019**, *131*, 958–968; c) Z. Zhou, J. Song, R. Tian, Z. Yang, G. Yu, L. Lin, G. Zhang, W. Fan, F. Zhang, G. Niu, L. Nie, X. Chen, *Angew. Chem. Int. Ed.* **2017**, *56*, 6492–6496; *Angew. Chem.* **2017**, *129*, 6592–6596; d) C. Yang, Y. Li, M. Du, Z. Chen, *J. Drug Targeting* **2019**, *27*, 33–50; e) H. Cheng, R.-R. Zheng, G.-L. Fan, J.-H. Fan, L.-P. Zhao, X.-Y. Jiang, B. Yang, X.-Y. Yu, S.-Y. Li, X.-Z. Zhang, *Biomaterials* **2019**, *188*, 1–11.
- [3] a) T. J. Dougherty, C. J. Gomer, B. W. Henderson, G. Jori, D. Kessel, M. Korbelik, J. Moan, Q. Peng, *J. Natl. Cancer Inst.* **1998**, *90*, 889–905; b) J. F. Lovell, T. W. B. Liu, J. Chen, G. Zheng, *Chem. Rev.* **2010**, *110*, 2839–2857; c) S. S. Lucky, K. C. Soo, Y. Zhang, *Chem. Rev.* **2015**, *115*, 1990–2042; d) G. Yu, T.-Y. Cen, Z. He, S.-P. Wang, Z. Wang, X.-W. Ying, S. Li, O. Jacobson, S. Wang, L. Wang, L. Lin, R. Tian, Z. Zhou, Q. Ni, X. Li, X. Chen, *Angew. Chem. Int. Ed.* **2019**, *58*, 8799–8803; *Angew. Chem.* **2019**, *131*, 8891–8895; e) L. Shen, Y. Huang, D. Chen, F. Qiu, C. Ma, X. Jin, X. Zhu, G. Zhou, Z. Zhang, *Theranostics* **2017**, *7*, 4537–4550; f) V. Shanmugam, S. Selvakumar, C.-S. Yeh, *Chem. Soc. Rev.* **2014**, *43*, 6254–6287; g) T. Guo, Y. Wu, Y. Lin, X. Xu, H. Lian, G. Huang, J. Z. Liu, X. Wu, H. H. Yang, *Small* **2018**, *14*, 1702815; h) H. Wang, Z. Liu, S. Wang, C. Dong, X. Gong, P. Zhao, J. Chang, *ACS Appl. Mater. Interfaces* **2014**, *6*, 3219–3225; i) Y. Jiang, X. Pang, R. Liu, Q. Xiao, P. Wang, A. W. Leung, Y. Luan, C. Xu, *ACS Appl. Mater. Interfaces* **2018**, *10*, 31674–31685; j) Y. Zhang, S. Bo, T. Feng, X. Qin, Y. Wan, S. Jiang, C. Li, J. Lin, T. Wang, X. Zhou, Z.-X. Jiang, P. Huang, *Adv. Mater.* **2019**, *31*, 1806444; k) C. Mao, F. Li, Y. Zhao, W. Debinski, X. Ming, *Theranostics* **2018**, *8*, 6274–6290.
- [4] a) B. Ding, S. Shao, C. Yu, B. Teng, M. Wang, Z. Cheng, K. L. Wong, P. A. Ma, J. Lin, *Adv. Mater.* **2018**, *30*, 1802479; b) Z. Yu, Q. Sun, W. Pan, N. Li, B. Tang, *ACS Nano* **2015**, *9*, 11064–11074; c) S. Wang, W. Yang, J. Cui, X. Li, Y. Dou, L. Su, J. Chang, H. Wang, X. Li, B. Zhang, *Biomater. Sci.* **2016**, *4*, 338–345; d) S. Wang, L. Zhang, C. Dong, L. Su, H. Wang, J. Chang, *Chem. Commun.* **2015**, *51*, 406–408; e) S. Veerananarayanan, M. S. Mohamed, A. C. Poulouse, M. Rinya, Y. Sakamoto, T. Maekawa, D. S. Kumar, *Theranostics* **2018**, *8*, 5231–5245.
- [5] a) N. Gong, X. Ma, X. Ye, Q. Zhou, X. Chen, X. Tan, S. Yao, S. Huo, T. Zhang, S. Chen, X. Teng, X. Hu, J. Yu, Y. Gan, H. Jiang, J. Li, X.-J. Liang, *Nat. Nanotechnol.* **2019**, *14*, 379–387; b) L.-S. Lin, T. Huang, J. Song, X.-Y. Ou, Z. Wang, H. Deng, R. Tian, Y. Liu, J.-F. Wang, Y. Liu, G. Yu, Z. Zhou, S. Wang, G. Niu, H.-H. Yang, X. Chen, *J. Am. Chem. Soc.* **2019**, *141*, 9937–9945; c) L. S. Lin, J. Song, L. Song, K. Ke, Y. Liu, Z. Zhou, Z. Shen, J. Li, Z. Yang, W. Tang, G. Niu, H. H. Yang, X. Chen, *Angew. Chem. Int. Ed.* **2018**, *57*, 4902–4906; *Angew. Chem.* **2018**, *130*, 4996–5000; d) G. Huang, H. Chen, Y. Dong, X. Luo, H. Yu, Z. Moore, E. A. Bey, D. A. Boothman, J. Gao, *Theranostics* **2013**, *3*, 116–126; e) L.-H. Fu, C. Qi, J. Lin, P. Huang, *Chem. Soc. Rev.* **2018**, *47*, 6454–6472; f) P. Liu, Y. Wang, L. An, Q. Tian, J. Lin, S. Yang, *ACS Appl. Mater. Interfaces* **2018**, *10*, 38833–38844; g) C. Y. Sun, Z. Cao, X. J. Zhang, R. Sun, C. S. Yu, X. Yang, *Theranostics* **2018**, *8*, 2939–2953; h) X. Wan, H. Zhong, W. Pan, Y. Li, Y. Chen, N. Li, B. Tang, *Angew. Chem. Int. Ed.* **2019**, <https://doi.org/10.1002/anie.201907388>; *Angew. Chem.* **2019**, <https://doi.org/10.1002/ange.201907388>.
- [6] a) H. Ranji-Burachaloo, P. A. Gurr, D. E. Dunstan, G. G. Qiao, *ACS Nano* **2018**, *12*, 11819–11837; b) Y. Dai, Z. Yang, S. Cheng, Z. Wang, R. Zhang, G. Zhu, B. C. Yung, R. Tian, O. Jacobson, C. Xu, Q. Ni, J. Song, X. Sun, G. Niu, X. Chen, *Adv. Mater.* **2018**, *30*, 1704877; c) L. Zhang, S.-S. Wan, C.-X. Li, L. Xu, H. Cheng, X.-Z. Zhang, *Nano Lett.* **2018**, *18*, 7609–7618; d) P. Ma, H. Xiao, C. Yu, J. Liu, Z. Cheng, H. Song, X. Zhang, C. Li, J. Wang, Z. Gu, J. Lin, *Nano Lett.* **2017**, *17*, 928–937; e) T. Zhu, L. Shi, C. Yu, Y. Dong, F. Qiu, L. Shen, Q. Qian, G. Zhou, X. Zhu, *Theranostics* **2019**, *9*, 3293–3307; f) L.-H. Fu, C. Qi, Y.-R. Hu, J. Lin, P. Huang, *Adv. Mater.* **2019**, *31*, 1808325; g) Y. Liu, W. Zhen, Y. Wang, J. Liu, L. Jin, T. Zhang, S. Zhang, Y. Zhao, S. Song, C. Li, *Angew. Chem. Int. Ed.* **2019**, *58*, 2407–2412; *Angew. Chem.* **2019**, *131*, 2429–2434.
- [7] a) G. Saravanakumar, J. Kim, W. J. Kim, *Adv. Sci.* **2017**, *4*, 1600124; b) S. Wang, Z. Wang, G. Yu, Z. Zhou, O. Jacobson, Y. Liu, Y. Ma, F. Zhang, Z. Y. Chen, X. Chen, *Adv. Sci.* **2019**, *6*, 1801986; c) L. H. Liu, W. X. Qiu, B. Li, C. Zhang, L. F. Sun, S. S. Wan, L. Rong, X. Z. Zhang, *Adv. Funct. Mater.* **2016**, *26*, 6257–6269; d) Y. Yuan, J. Liu, B. Liu, *Angew. Chem. Int. Ed.* **2014**, *53*, 7163–7168; *Angew. Chem.* **2014**, *126*, 7291–7296; e) F. Zhou, B. Feng, T. Wang, D. Wang, Z. Cui, S. Wang, C. Ding, Z. Zhang, J. Liu, H. Yu, *Adv. Funct. Mater.* **2017**, *27*, 1703674; f) Y. Dou, Y. Liu, F. Zhao, Y. Guo, X. Li, M. Wu, J. Chang, C. Yu, *Theranostics* **2018**, *8*, 5870–5889; g) X. Liu, J. Xiang, D. Zhu, L. Jiang, Z. Zhou, J. Tang, X. Liu, Y. Huang, Y. Shen, *Adv. Mater.* **2016**, *28*, 1743–1752.
- [8] a) D. Trachootham, J. Alexandre, P. Huang, *Nat. Rev. Drug Discovery* **2009**, *8*, 579; b) M. Ye, Y. Han, J. Tang, Y. Piao, X. Liu, Z. Zhou, J. Gao, J. Rao, Y. Shen, *Adv. Mater.* **2017**, *29*, 1702342; c) X. Xu, P. E. Saw, W. Tao, Y. Li, X. Ji, S. Bhasin, Y. Liu, D. Ayyash, J. Rasmussen, M. Huo, J. Shi, O. C. Farokhzad, *Adv. Mater.* **2017**, *29*, 1700141; d) F. Fan, Y. Yu, F. Zhong, M. Gao, T. Sun, J. Liu, H. Zhang, H. Qian, W. Tao, X. Yang, *Theranostics* **2017**, *7*, 1290–1302; e) B. C. Dickinson, C. J. Chang, *Nat. Chem. Biol.* **2011**, *7*, 504–511.
- [9] a) S. Wang, G. Yu, Z. Wang, O. Jacobson, R. Tian, L. S. Lin, F. Zhang, J. Wang, X. Chen, *Adv. Mater.* **2018**, *30*, 1803926; b) X. Hu, G. Liu, Y. Li, X. Wang, S. Liu, *J. Am. Chem. Soc.* **2015**, *137*, 362–368; c) X. Hu, S. Zhai, G. Liu, D. Xing, H. Liang, S. Liu, *Adv. Mater.* **2018**, *30*, 1706307; d) H. Liang, Z. Zhou, R. Luo, M. Sang, B. Liu, M. Sun, W. Qu, F. Feng, W. Liu, *Theranostics* **2018**, *8*, 5059–5071; e) Y. Xia, T. Xu, M. Zhao, L. Hua, Y. Chen, C. Wang, Y. Tang, B. Zhu, *Int. J. Mol. Sci.* **2018**, *19*, 3582.
- [10] a) D. Guo, S. Xu, Y. Huang, H. Jiang, W. Yasen, N. Wang, Y. Su, J. Qian, J. Li, C. Zhang, X. Zhu, *Biomaterials* **2018**, *177*, 67–77; b) J. Li, W. Ke, L. Wang, M. Huang, W. Yin, P. Zhang, Q. Chen, Z. Ge, *J. Controlled Release* **2016**, *225*, 64–74; c) H. Jin, M. Sun, L. Shi, X. Zhu, W. Huang, D. Yan, *Biomater. Sci.* **2018**, *6*, 1403–1413; d) J. Li, Y. Li, Y. Wang, W. Ke, W. Chen, W. Wang, Z. Ge,

- Nano Lett.* **2017**, *17*, 6983–6990; e) L. Hua, Z. Wang, L. Zhao, H. Mao, G. Wang, K. Zhang, X. Liu, D. Wu, Y. Zheng, J. Lu, R. Yu, H. Liu, *Theranostics* **2018**, *8*, 5088–5105; f) P. Sun, N. Wang, X. Jin, X. Zhu, *ACS Appl. Mater. Interfaces* **2017**, *9*, 36675–36687.
- [11] a) Y. Wang, K. Zhou, G. Huang, C. Hensley, X. Huang, X. Ma, T. Zhao, B. D. Sumer, R. J. DeBerardinis, J. Gao, *Nat. Mater.* **2014**, *13*, 204–212; b) Y. Wang, C. Wang, Y. Li, G. Huang, T. Zhao, X. Ma, Z. Wang, B. D. Sumer, M. A. White, J. Gao, *Adv. Mater.* **2017**, *29*, 1603794.
- [12] a) E. Blanco, E. A. Bey, C. Khemtong, S. G. Yang, J. Setti-Guthi, H. Chen, C. W. Kessinger, K. A. Carnevale, W. G. Bornmann, D. A. Boothman, J. Gao, *Cancer Res.* **2010**, *70*, 3896–3904; b) X. Ma, X. Huang, G. Huang, L. Li, Y. Wang, X. Luo, D. A. Boothman, J. Gao, *Adv. Healthcare Mater.* **2014**, *3*, 1210–1216.
- [13] a) S. Wang, Z. Zhou, G. Yu, N. Lu, Y. Liu, Y. Dai, X. Fu, J. Wang, X. Chen, *ACS Appl. Mater. Interfaces* **2018**, *10*, 28382–28389; b) S. Wang, Z. Zhou, Z. Wang, Y. Liu, O. Jacobson, Z. Shen, X. Fu, Z. Y. Chen, X. Chen, *Small* **2019**, *15*, 1900691.
- [14] a) S. Wang, P. Huang, X. Chen, *Adv. Mater.* **2016**, *28*, 7340–7364; b) L. An, X. Wang, X. Rui, J. Lin, H. Yang, Q. Tian, C. Tao, S. Yang, *Angew. Chem. Int. Ed.* **2018**, *57*, 15782–15786; *Angew. Chem.* **2018**, *130*, 16008–16012; c) Q. Jin, Y. Deng, X. Chen, J. Ji, *ACS Nano* **2019**, *13*, 954–977; d) S. Wang, J. Lin, Z. Wang, Z. Zhou, R. Bai, N. Lu, Y. Liu, X. Fu, O. Jacobson, W. Fan, J. Qu, S. Chen, T. Wang, P. Huang, X. Chen, *Adv. Mater.* **2017**, *29*, 1701013.

Manuscript received: July 19, 2019

Accepted manuscript online: August 19, 2019

Version of record online: September 3, 2019